Commun Transp Res

Research Article

# Capacity Drop as a Phase Transition: An Analytical Model via Stochastic Disturbance Propagation

Xiaohui Zhang[1, 2, 3], Jie Sun[2], Jian Sun[2,✉], Yunpeng Wang[4]

Cite this article: https://doi.org/10.26599/COMMTR.2026.9640065

**ABSTRACT:** Understanding and mitigating capacity drop is crucial for efficient transportation systems, yet an explicit link from microscopic interactions to this macroscopic phenomenon remains unclear. Drawing on phase transition and critical phenomena theory, this study models the capacity drop as a collective response to speed disturbances that originate from microscopic stochastic interactions and propagate across the platoon at critical density. Specifically, by inducing speed disturbances into the equilibrium traffic, we first develop the response function of mean flow under disturbances. To quantify the effective range of disturbance propagation, we introduce the correlation length, defined as the distance over which the correlation between disturbances remains significant before decaying. With the maximum correlation length indicating the critical density, we thus derive the capacity drop as the response function of the mean flow within this length. Building on this formulation, we propose an analytical model for capacity drop considering the effects of disturbance propagation, based on the equilibrium traffic flow model—the leader-follower conditional distribution based stochastic traffic model (LFCD-STM) developed in our previous work. The proposed capacity drop model is validated using Zen and I-24 MOTION datasets, demonstrating satisfactory performance with all relative errors in flow rates and critical density below 5%. Overall, this work provides a foundational understanding and analytical modeling of capacity drop from the perspective of speed disturbance propagation, offering valuable insights that help develop traffic management strategies and guide the advancement of connected and automated vehicle technologies.

**KEYWORDS:** capacity drop; phase transition; disturbance propagation; correlation length; stochastic traffic modeling

Just Accepted

## 1 Introduction

Capacity drop, defined as the outflow from a bottleneck under congestion (queue discharge flow rate, QDF) being smaller than the maximum possible outflow under free-flow conditions (capacity), have been observed and investigated in numerous empirical studies (Banks, 1991; Bertini and Leal, 2005; Cassidy and Bertini, 1999; Edie, 1961; Srivastava and Geroliminis, 2013). Analogous to a phase transition (Chowdhury et al., 2000), it marks the transition from free flow to congested flow where the queue forms, resulting in increased travel time, crash risks, energy consumptions and emissions. This complex phenomenon also leads to the inverse lambda shape of the fundamental diagram, in which the flow-density relation is not unique for a certain range of densities (i.e., a higher flow for free traffic and a lower one for congested traffic) (Treiber and Kesting, 2013). Moreover, the magnitude of capacity drop, typically ranging between 5% to 30%, is not consistent and varies even at the same location due to the stochastic nature of traffic flow (Brilon et al., 2005; Hall and Agyemang-Duah, 1991).

Extensive efforts have been made to understand the underlying mechanism of capacity drop, which suggest that capacity drop arises from lane-changes (LC) (Laval and Daganzo, 2006) and car-following (CF) behaviors (Treiber et al., 2006). Specifically, it is conjectured that limited acceleration capability during LCs creates voids, reducing the discharge flow rate of bottlenecks (Cassidy and Rudjanakanoknad, 2005; Chen and Ahn, 2018; Leclercq et al., 2011; Oh and Yeo, 2015). On the other hand, variable CF behaviors that contribute to capacity drop are further categorized as inter-driver spread, intra-driver spread, and stochasticity. Inter-driver spread refers to differences in acceleration among driver-vehicle units (Papageorgiou et al., 2008), while intra-driver spread involves drivers adjusting CF behaviors in different traffic conditions (Nishinari et al., 2003). Stochastic effects, stemming from human error or multiple sources of heterogeneities, introduce random fluctuations and thus disrupt traffic flow (Yuan et al., 2019). Incorporating these behavioral mechanisms, many models have been developed to reproduce the capacity drop through simulation (see details in the Literature Review).

Despite empirical investigations and simulation replications of capacity drop in previous studies, an analytical model that explicitly connects microscopic behaviors to macroscopic capacity drop remains lacking. Closing this gap is essential for a deeper understanding of traffic flow physics and for designing effective control strategies in alleviating traffic congestion via connected and automated vehicles.

To this end, we treat capacity drop as a phase transition, analyzing it through the lens of stochastic disturbance propagation, see Fig.1. Regardless of whether the initial trigger of capacity drop is a lateral cut-in (LC) or longitudinal braking (CF), the macroscopic transition to a congested flow is ultimately determined by whether these local perturbations dissipate or amplify as they propagate along the platoon

[1] Institute of Smart City and Intelligent Transportation, Institute of Urban Rail Transportation, Southwest Jiaotong University, Chengdu 611756, China. [2] Department of Traffic Engineering & Key Laboratory of Road and Traffic Engineering of Ministry of Education, Tongji University, Shanghai 201804, China. [3] National Engineering Research Center of Road Safety Control Technology, Beijing 100176, China. [4] School of Transportation Science and Engineering, Beihang University, Beijing 102206, China.

✉ Corresponding author. E-mail: sunjian@tongji.edu.cn

Received: June 23, 2026; Revised: August 31, 2026; Accepted: October 29, 2029

© The Author(s) 2026. This is an open access article under the terms of the Creative Commons Attribution 4.0 International License (CC BY 4.0, http://creativecommons.org/licenses/by/4.0/).

(Castillo, 2001; Chen et al., 2019; Han and Ahn, 2018). By focusing on the stochastic dynamics of disturbance propagation, mainly shaped by longitudinal leader-follower interactions, our framework provides a parsimonious yet effective abstraction that characterizes the essential physics of capacity drop. This perspective is deeply rooted in the theory of phase transitions and critical phenomena (Nishimori and Ortiz, 2010), where the sudden change in macroscopic property (i.e., capacity drop) occurs as the disturbance propagates extensively at the critical point (i.e., critical density), making the system respond collectively.

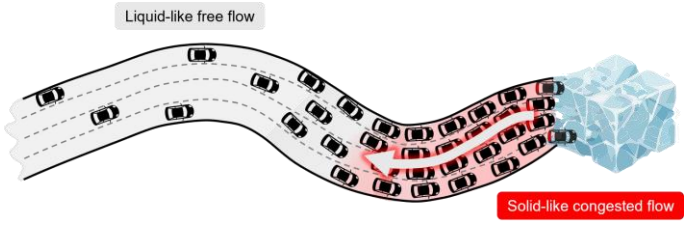



**Fig. 1.** Capacity drop as a phase transition with widespread disturbances.

Generally, the disturbance propagation has been investigated in linear string stability analysis to interpret the traffic oscillation (Chandler et al., 1958; Herman et al., 1959; Sun et al., 2018, 2020; Swaroop and Hedrick, 1996; Wilson and Ward, 2011; X. Zhang and Jarrett, 1997; X. Zhang et al., 2024). However, the commonly used frequency domain based methods make it opaque to understand the disturbance propagation. In addition, these stability analysis methods rely on analytical CF models, which impose strong assumptions on the microscopic interaction with specific CF rules. Furthermore, it is challenging to theoretically assess the impact of sufficiently large disturbances, such as inconsiderate hard braking or LC. More importantly, the explicit connection between the microscopic disturbances and macroscopic capacity drop remains lacking.

To bridge these gaps, this study investigates the impact of disturbance propagation on the emergence of capacity drop and aims to provide an analytical link between them. To this end, we formulate the capacity drop as a collective response to widespread disturbances at the critical density. Specifically, we first introduce speed disturbances into the equilibrium traffic flow and develop the response function of mean flow under disturbances. To quantify the effective range of disturbance propagation, we employ the concept of correlation length from the phase transition and critical phenomena theory, defined as the distance over which the correlation between disturbances remains significant before decaying. The maximum correlation length, which marks the critical point, further allows us to obtain the capacity drop at the critical density by restricting the response function within this length.

Following this general formulation, we propose an analytical capacity drop model from the perspective of disturbance propagation, based on a probabilistic equilibrium traffic flow model developed in our previous work (X. Zhang et al., 2025). This equilibrium model, referred to as leader-follower conditional distribution based stochastic traffic model (LFCD-STM), represents the longitudinal interaction as a conditional distribution of speed and then derives the stochastic flow-density relation in equilibrium through Markov chain modeling. By extending the LFCD-STM to non-equilibrium states, we analytically derive the capacity drop from the perspective of disturbance propagation. The major contributions are summarized as follows:

- Leveraging phase transition and critical phenomena theory, we innovatively formulate the capacity drop as a collective response to widespread speed disturbances, confined within the maximum correlation length of propagation at the critical density.
- Extending the micro-macroscopic LFCD-STM to non-equilibrium states, we derive the response function of mean flow under disturbances at the critical density through perturbative expansion, analytically connecting microscopic stochastic disturbances to macroscopic capacity drop.
- Using Zen and I-24 MOTION datasets, we rigorously validate the proposed capacity drop model, showing satisfactory performance with all relative errors in estimated flow rates and critical density under 5%.

Moreover, we examine the sensitivity of parameters in the developed capacity drop model. The remainder of this paper is organized as follows: Section 2 reviews the related literature; Section 3 presents the general formulation; Section 4 details the derivation of capacity drop at critical density, based on the LFCD-STM; Section 5 calibrates and validates the proposed model using the Zen and I-24 MOTION datasets; Section 6 conducts sensitivity analysis; and Section 7 summarizes the main findings.

## 2 Literature review

Capacity drop refers to the phenomenon that the discharge flow observed during congested conditions is lower than the capacity under free-flow conditions. Early observations by Hall and Agyemang-Duah (1991) reported a 6% capacity drop at an on-ramp bottleneck, providing one of the first empirical confirmations of this phenomenon. Later in the decade, Cassidy and Bertini (1999) observed capacity drops between 8% and 10% at bottlenecks formed by lane drops and horizontal curves. Cassidy and Rudjanakanoknad (2005) also found capacity drops ranging from 8.3% to 14.7% at on-ramp bottlenecks. Shortly after, Chung et al. (2007) observed capacity drops from 3% to 18% across three active bottlenecks (on-ramp merge, lane drop, and horizontal curve). Notably, they found that even at a single location, capacity drop could vary from 8% to 18%. In addition, Srivastava and Geroliminis (2013) noted a capacity drop of approximately 15% at an on-ramp bottleneck. More recent research based on high-resolution trajectory data in a weaving section, extracted from videos recorded by unmanned aerial vehicles, reported capacity drops ranging from 8.7% to 22.9% (Han et al., 2025). The wide range of observed magnitudes not only between sites but also at the same location underscores the stochastic nature of capacity drop phenomenon. While capacity drop magnitudes exhibit apparent variations, the critical density associated with it is observed to be more stable (Cassidy and Bertini, 1999; Srivastava and Geroliminis, 2013). Chung et al. (2007) studied three bottleneck sites (I-805 North, SR-24 West, and Gardiner Expressway West) for the relationship between density and capacity drop and found the critical densities that coincided with capacity drops were similar across bottlenecks.

To understand the puzzling capacity drop phenomenon, several behavioral mechanisms have been proposed, which reveals that LC maneuvers and variable CF behaviors are key contributors. LC has long been a focus given its direct impact on traffic flow, which creates voids due to bounded acceleration and thus reduces the discharge flow rate. Laval and Daganzo (2006) combined the multi-lane kinematic wave

Just Accepted

theory with the constrained-motion model to capture the limited ability to accelerate after LCs. This hybrid model reproduced the capacity drop of the active bottleneck via numerical experiments. Chen and Ahn (2018) proposed a physical moving bottleneck approach to model the impact of LC vehicles' bounded acceleration, utilizing the kinematic wave theory and Newell's simplified CF model. Capacity drop was then estimated through numerical simulations in three types of extended bottlenecks (i.e., merge, diverge, and weave). Moreover, Jin (2017) developed an extension of the Lighthill-Whitham-Richards (LWR) model considering the effect of bounded acceleration (BA-LWR), which directly incorporates acceleration limits into the governing equations.

The CF behaviors that contribute to capacity drop can be broadly categorized into inter-driver heterogeneity, intra-driver variability, and stochasticity. Inter-driver heterogeneity refers to variations among drivers. Ngoduy and Liu (2007) delineated separate LWR equations for each driver class, namely the multi-class LWR model (MC-LWR), interlinked through the fundamental diagram, to capture such heterogeneities macroscopically. Yuan et al. (2017) demonstrated how differences in acceleration between successive vehicles can prevent timely gap closure, diminishing the bottleneck throughput. Intra-driver variability suggests that driver behavior varies with traffic conditions. Drivers may choose longer time headways in congestion compared to free-flow conditions, as proposed by the variance-driven time headway theory (Treiber et al., 2006), which qualitatively reproduces capacity drops in numerical simulations. Additionally, incorporating acceleration, deceleration and coasting phases, the multi-phase CF theory has been developed to model the capacity drop (H.M. Zhang and Kim, 2005). Moreover, Nishinari et al. (2003) ascribed the capacity drop to the empirically observed resignation effect, where the time gap becomes larger after passing congested traffic. Chen et al. (2014) also demonstrated that discharge rate reductions can occur due to less aggressive driver characteristics. The stochasticity from multiple sources of heterogeneity and human error is another essential ingredient of capacity drop. Qian et al. (2017) used stochastic differential equations with discrete speed states based on the gas-kinetic theory, showing how stochastic noise can produce the discontinuity in fundamental diagram consistent with capacity drop. Yuan et al. (2019) modeled driver acceleration errors as Geometric Brownian motion, simulating different capacity drop magnitudes across varying traffic situations. In the field of physics, the cellular automaton (CA) model for freeway traffic with the random effects can also reproduce capacity drop to some extent (Kerner et al., 2011).

We summarize representative studies in Table 1. Overall, most studies model the capacity drop through simulations, while the analytical tractability is absent yet critical for the efficient prediction and optimization of the traffic flow. This study aims to derive capacity drop by adopting the perspective of disturbance propagation, which facilitates the incorporation of existing behavioral mechanisms into a cohesive analytical framework.

**Table 1.** Representative studies of capacity drop modeling.

| Mechanism | Study | Model | Stochasticity | Micro–macro link |
|---|---|---|---|---|
| **LC with bounded acceleration** | Laval and Daganzo (2006) | Kinematic wave + constrained motion | No | Macro / simulation |
| | Jin et al. (2015); Jin (2017) | BA-LWR | No | Macro / analytical |
| | Chen and Ahn (2018) | Newell CF + moving bottleneck | No | Micro→ macro / simulation |
| **Intra-driver variation** | H.M. Zhang and Kim (2005) | Multiphase CF | No | Micro→ macro / simulation |
| | Treiber et al. (2006) | IDM + variable headway | No | Micro→ macro / simulation |
| | Chen et al. (2014) | Newell CF + aggressiveness | No | Micro→ macro / simulation |
| **Inter-driver spread** | Ngoduy and Liu (2007) | Multiclass LWR | No | Macro / simulation |
| | Yuan et al. (2017) | Extended Newell CF | No | Micro→ macro / simulation |
| **Stochasticity** | Kerner et al. (2011) | Cellular automaton | Yes | Micro→ macro / simulation |
| | Qian et al. (2017) | Discrete speed + SDE | Yes | Micro→ macro / simulation |
| | Yuan et al. (2019) | Brownian-motion CF | Yes | Micro→ macro / simulation |
| **Stochastic disturbance propagation** | **This study** | **LFCD-STM + response theory** | **Yes** | **Micro→ macro / analytical** |

## 3 General formulation

In this section, we present the overarching formulation of capacity drop from the perspective of disturbance propagation. Our basic idea is to analyze the macroscopic property of traffic flow under speed disturbances at critical density, synthesizing traffic flow theory and phase transition theory in statistical physics. In traffic flow theory, the capacity drop phenomenon refers to the abrupt reduction of capacity when density crosses a critical threshold. In statistical physics, such an abrupt change in macroscopic properties defines a phase transition, where fluctuations spread across the entire system at the critical point and the system responds collectively (Nishimori and Ortiz, 2010). We thus recast capacity drop as a phase transition driven by speed disturbance propagation. Regardless of whether the microscopic triggers are LC with bounded acceleration or variable CF behaviors, both generate speed disturbances that propagate upstream along the platoon (Castillo, 2001; Chen et al., 2019; Han and Ahn, 2018; Treiber

Just Accepted

and Kesting, 2013). At the critical density, these disturbances span nearly the entire platoon, inducing a collective response that manifests as the macroscopic capacity drop.

Building on this core idea, we formulate the capacity drop as a response function (Marini Bettolo Marconi et al., 2008) of mean flow at the critical density $k_c$ under disturbances $\boldsymbol{\mathcal{E}}$ with respect to equilibrium free-flow capacity:

$$\mathrm{E}[Q|\boldsymbol{\mathcal{E}}] = \left(1 - \delta_{k_c}\right)\mathrm{E}[Q|\boldsymbol{\mathcal{E}} = \mathbf{0}] \quad (1)$$

where $\delta_{k_c}$ is the expected capacity drop magnitude, $\mathrm{E}[Q|\boldsymbol{\mathcal{E}} = \mathbf{0}]$ is the equilibrium capacity. The mathematical formulation is developed in a stochastic manner, accounting for the stochastic nature of traffic flow as evidenced by empirical studies (Coifman, 2015; Daganzo, 2002; Treiber et al., 2006). To avoid ambiguity, we distinguish random variables by using upper case letters, including the equilibrium speed and flow of the platoon $V_e$, $Q_e$, the average speed of the platoon $\overline{V}$, the flow of the platoon $Q$, the speed of $i$th vehicle in the platoon $V_i$, the speed disturbance of $i$th vehicle in the platoon $\mathcal{E}_i$ (deviation from the average speed of the platoon, $\mathcal{E}_i = V_i - \overline{V}$) and the vector of speed disturbances along the platoon $\boldsymbol{\mathcal{E}} = (\mathcal{E}_0, \mathcal{E}_1, \cdots, \mathcal{E}_n)$. Appendix A summarizes the notations used throughout this paper.

The formulation in Eq. (1) captures the capacity drop at the critical density through several interconnected concepts. The equilibrium traffic flow $\mathrm{E}[Q|\boldsymbol{\mathcal{E}} = \mathbf{0}]$ is the undisturbed baseline, i.e., $\mathrm{E}[Q|\boldsymbol{\mathcal{E}} = \mathbf{0}] = \mathrm{E}[Q_e]$, representing the capacity the system would sustain without any disturbance. The mean flow response $\mathrm{E}[Q|\boldsymbol{\mathcal{E}}]$ reflects how this baseline is collectively degraded as speed disturbances propagate through the platoon. The capacity drop magnitude $\delta_{k_c}$ emerges as the gap between the two, evaluated at the critical density $k_c$ where disturbances span the platoon. To pinpoint $k_c$ and the spatial range of this collective response, we draw on the correlation length from phase transition theory (Hohenberg and Halperin, 1977), which measures how far disturbances remain correlated across the platoon and peaks at the critical point.

## 4 The capacity drop model

In this section, we derive the capacity drop model by capturing disturbance propagation effects with the proposed formulation, as illustrated in Fig. 2. Specifically, using the LFCD-STM developed in our previous work (X. Zhang et al., 2025) as the equilibrium basis, we perform a perturbative expansion at both micro- and macroscopic levels to derive the disturbance propagation equation and assess the mean flow response to disturbances. The effective spatial range of disturbance propagation is further quantified by correlation length. Within the maximum correlation length, the capacity drop is derived as the response function of mean flow at the identified critical density. The derivation is developed under Markovian leader–follower interactions, statistical homogeneity under a given local traffic state, and local quasi-stationarity, with these assumptions further specified and justified at the corresponding modeling steps.

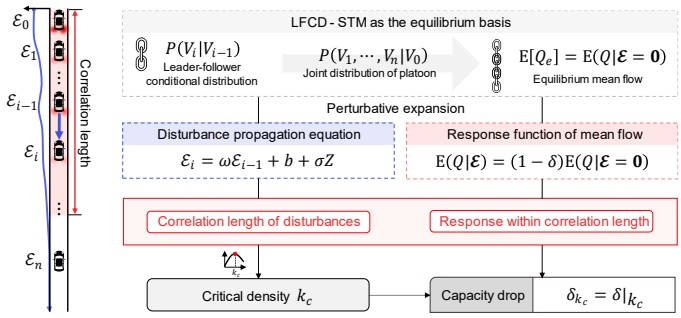



**Fig. 2.** Modeling framework of capacity drop.

### 4.1. *Equilibrium basis*

To lay the foundation for analytical modeling of capacity drop, we use the LFCD-STM developed in our previous work as the equilibrium basis, which provides a general micro-macroscopic approach for stochastic traffic flow modeling. To be specific, the LFCD-STM analytically links the stochastic fundamental diagram (SFD) with the microscopic driving behavior. The microscopic interaction is first defined as the conditional distribution of speed for each leader-follower pair, which is compatible with classic CF models according to the Brownian dynamics. By aggregating these longitudinal interactions with Markov chain modeling, we obtain the joint distribution of vehicle speeds representing the collective behavior of platoon. With equilibrium conditions, we further derive the distribution of equilibrium speed with respect to density and the mean flow-density relation with its variance. Based on this general micro-macroscopic link, we derive the concrete SFD model with a specific conditional distribution for longitudinal interaction using the maximum entropy approach.

Formally, the longitudinal interaction is characterized by the conditional distribution of the follower's speed $V_i$ given the leader's speed $V_{i-1}$, i.e., $P(V_i|V_{i-1})$, where $P(V_i|V_{i-1}) = P(V_i|V_{i-1}, \cdots, V_0)$, employing the widely adopted assumption that the following vehicle mainly reacts to its immediate leader (Brackstone and McDonald, 1999). For a closed-form and general behavior, we directly model the conditional distribution using the maximum entropy approach. The core idea is to incorporate prior knowledge through expectation constraints and then select the least-biased distribution, which has been rigorously proven to possess the maximum entropy and to yield an exponential-family distribution as a mathematical necessity rather than a pre-defined assumption (Csiszar, 1991; Jaynes, 1957, 1982; Shore and Johnson, 1980). As shown in Eq. (2), the structure within the exponential is determined by carefully selected characteristic functions corresponding to the expectation constraints, which measure the local interaction with the leader $f_{int}$, the subject vehicle's speed $f_{own}$, and its speed fluctuation relative to the platoon mean $f_{flu}$.

$$\begin{aligned} P(V_i = v_i|V_{i-1} = v_{i-1}) &\propto e^{-(\lambda_1 f_{int} + \lambda_2 f_{own} + \lambda_3 f_{flu})} \\ &= e^{-[\lambda_1 (v_i - v_{i-1})^2 + \lambda_2 v_i + \lambda_3 (v_i - \bar{v})^2]} \end{aligned} \quad (2)$$

Specifically, as per the work in flocks of birds (Bialek et al., 2012, 2014), the interaction term is defined as $f_{int} = (v_i - v_{i-1})^2$ to quantify the speed difference between the leader and follower and describe the tendency of the follower to adjust its speed to follow the leader; the speed term $f_{own} = v_i$ is the speed of the follower, standing for its own state which dominates the distribution once other terms are zero; and the fluctuation term $f_{flu} = (v_i - \bar{v})^2$ measures individual vehicle's speed fluctuation compared to the mean speed of platoon $\bar{v}$. Here, $\bar{v}$ serves as an external environmental parameter, characterizing the

Just Accepted

ambient traffic in which each leader-follower pair is embedded.

Moreover, the associated coefficients $\lambda_1, \lambda_2, \lambda_3$, termed Lagrange multipliers following the standard convention of the maximum entropy approach, are not fixed but are calibrated via maximum likelihood estimation using trajectory data and vary with spacings (and thus traffic density). As revealed by empirical analyses of NGSIM and HighD datasets, $\lambda_1$ and $\lambda_2$ exhibit a logarithmic relationship with spacing $s$/density $k$, where $\eta, \theta, \alpha, \beta$ are parameters, see Eqs. (3)-(4) and our previous work for details (X. Zhang et al., 2025). This data-driven formulation therefore yields the leader-follower conditional distribution that adapts naturally across traffic states.

$$\lambda_1 = -\eta \ln s + \theta = \eta \ln k + \theta \tag{3}$$

$$\lambda_2 = -\alpha \ln s + \beta = \alpha \ln k + \beta \tag{4}$$

Notably, the proposed leader-follower conditional distribution is formulated in a stationary form without explicit time evolution, where the transient adaptation process is approximated as a sequence of stationary states. This quasi-stationary assumption, commonly used in non-equilibrium statistical physics to characterize metastable regimes (Cáceres, 2017). In this regime, where traffic operates near capacity, drivers adjust to leader behavior over short response intervals, while traffic breakdown develops more slowly as disturbances need to propagate along the platoon before eventually triggering a phase transition to congestion. These microscopic adjustments occur much faster than the macroscopic evolution, the leader-follower interaction can thus be reasonably approximated as locally stationary. Under this standard assumption, temporal effects such as reaction delays are embedded in the empirical conditional statistics (C. Zhang et al., 2024; C. Zhang et al., 2026), which primarily manifests as increased conditional variability.

Based on this probabilistic model of local interaction $P(V_i|V_{i-1})$, we model the collective behavior of the whole platoon as a joint distribution. Here, a platoon is defined as the ordered sequence of vehicles in the same lane on a continuous and homogeneous road segment. Consider a section of single-lane highway where vehicle $i$ follows vehicle $(i-1)$, the joint distribution of vehicle speeds in the system is $P(V_1, \cdots, V_n|V_0)$, where $n$ is the total number of vehicles in the study section and $V_0$ is the speed of the leading vehicle in the platoon. Using the chain rule in probability theory and the Markov assumption of longitudinal interactions, we have:

$$\begin{aligned} P(V_1, \cdots, V_n|V_0) &= \frac{P(V_0, V_1, \cdots, V_n)}{P(V_0)} \\ &= \frac{P(V_0)\prod_{i=1}^{n} P(V_i|V_{i-1}, \cdots, V_0)}{P(V_0)} \\ &= \frac{P(V_0)\prod_{i=1}^{n} P(V_i|V_{i-1})}{P(V_0)} \\ &= \prod_{i=1}^{n} P(V_i|V_{i-1}) \end{aligned} \tag{5}$$

Assuming homogenous leader-follower pairs, we substitute Eq. (2) into Eq. (5):

$$\begin{aligned} &P(V_1 = v_1, \cdots, V_n = v_n|V_0 = v_0) \\ &\propto e^{-[\sum_{i=1}^{n}\lambda_1(v_i - v_{i-1})^2 + \sum_{i=1}^{n}\lambda_2 v_i + \sum_{i=1}^{n}\lambda_3(v_i - \bar{v})^2]} \end{aligned} \tag{6}$$

Under equilibrium that every vehicle takes the same speed value simultaneously, we derive the distribution of the equilibrium speed $P(V_e)$, where $n = kl$, $k$ is the density, $l$ is the length of the study area and $v_{max}$ is the maximum speed:

$$\begin{aligned} P(V_e = v_e) &\propto P(V_1 = v_e, \cdots, V_n = v_e|V_0 = v_e) \\ &= \frac{e^{-\lambda_2 n v_e}}{\sum_{v_e=0}^{v_{max}} e^{-\lambda_2 n v_e}} = \frac{\lambda_2 kl e^{-\lambda_2 kl v_e}}{1 - e^{-\lambda_2 kl v_{max}}} \end{aligned} \tag{7}$$

Using $Q = kV$, the mean and variance of equilibrium flow $Q_e$ with respect to density $k$ are:

$$\mathrm{E}[Q_e] = k\mathrm{E}[V_e] = \frac{1}{\lambda_2 l} - \frac{k v_{max} e^{-\lambda_2 v_{max} kl}}{1 - e^{-\lambda_2 v_{max} kl}} \tag{8}$$

$$\mathrm{Var}[Q_e] = k^2\mathrm{Var}[V_e] = \frac{1}{{\lambda_2}^2 l^2} - \frac{k^2 {v_{max}}^2}{e^{-\lambda_2 v_{max} kl} + e^{\lambda_2 v_{max} kl} - 2} \tag{9}$$

Substituting Eq. (3) and Eq. (4) into Eq. (8) and Eq. (9), we have the complete maximum entropy distribution based SFD model, which is highly consistent with empirical results, as shown in Fig. 3:

$$\mathrm{E}[Q_e] = \frac{1}{(\alpha \ln k + \beta) l} - \frac{k v_{max} e^{-(\alpha \ln k + \beta) v_{max} kl}}{1 - e^{-v_{max} kl(\alpha \ln k + \beta)}} \tag{10}$$

$$\begin{aligned} &\mathrm{Var}[Q_e] \\ &= \frac{1}{(\alpha \ln k + \beta)^2 l^2} \\ &- \frac{k^2 {v_{max}}^2}{e^{-v_{max} kl(\alpha \ln k + \beta)} + e^{v_{max} kl(\alpha \ln k + \beta)} - 2} \end{aligned} \tag{11}$$

Overall, the LFCD-STM offers the baseline of equilibrium flow and provides an analytical approach to derive it from microscopic interactions. By focusing on the longitudinal interactions, which primarily characterize the propagation of disturbances, the LFCD-STM further enables extensions to approximate the non-equilibrium phenomenon of capacity drop by capturing the effects of propagating disturbances.

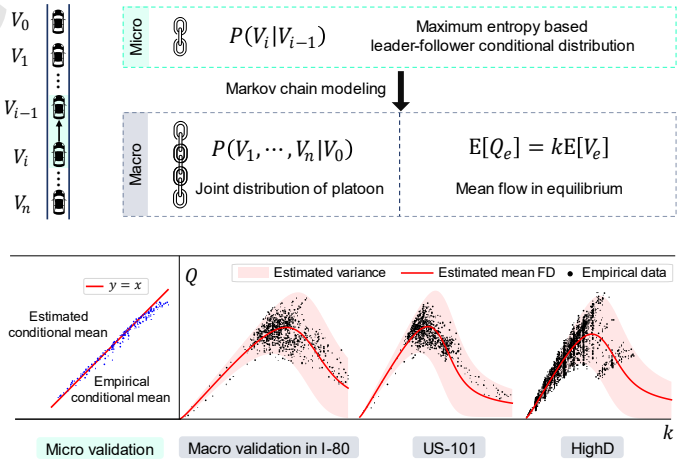



**Fig. 3.** The LFCD-STM developed in our previous work (X. Zhang et al., 2025).

### *4.2. Perturbative expansion*

To capture the effects of disturbance propagation, we perform the perturbative expansion on the LFCD-STM. Formally, the speed of each vehicle $V_i$ is decomposed into the average speed of the platoon $\overline{V}$ and the speed disturbance $\mathcal{E}_i$, i.e., $V_i = \overline{V} + \mathcal{E}_i$. Note that with this definition of speed disturbance, we have $\sum_i \mathcal{E}_i = 0$. By substituting the decomposition into the micro- and macro-level of LFCD-STM, we derive the disturbance propagation equation and response function of mean flow respectively.

#### *4.2.1. Disturbance propagation equation*

The disturbance propagates upstream along the platoon, mainly driven by the leader-follower interactions. Based on the leader-follower conditional distribution $P(V_i|V_{i-1})$ in the LFCD-STM, we derive the equation of speed disturbance propagation using perturbative

Just Accepted

expansion. Given a realization of the platoon average speed $\overline{V} = \bar{v}$ that is identical to all leader-follower pairs, we insert $V_i = \bar{v} + \varepsilon_i$ into the $P(V_i|V_{i-1})$ in Eq. (2):

$$P(V_i = \bar{v} + \varepsilon_i | V_{i-1} = \bar{v} + \varepsilon_{i-1}) \propto e^{-[\lambda_1(\varepsilon_i - \varepsilon_{i-1})^2 + \lambda_2(\bar{v}+\varepsilon_i) + \lambda_3 \varepsilon_i^2]} \tag{12}$$

It can be further simplified as the conditional distribution of $\mathcal{E}_i$ given $\mathcal{E}_{i-1}$:

$$P(\mathcal{E}_i = \varepsilon_i | \mathcal{E}_{i-1} = \varepsilon_{i-1}) \propto e^{-[\lambda_1(\varepsilon_i - \varepsilon_{i-1})^2 + \lambda_2 \varepsilon_i + \lambda_3 \varepsilon_i^2]} \tag{13}$$

Rearranging the quadratic exponent yields a Gaussian conditional distribution:

$$\begin{aligned} P(\mathcal{E}_i = \varepsilon_i | \mathcal{E}_{i-1} = \varepsilon_{i-1}) &\propto e^{-(\lambda_1+\lambda_3)\left[\varepsilon_i - \left(\frac{\lambda_1 \varepsilon_{i-1} - \frac{\lambda_2}{2}}{\lambda_1+\lambda_3}\right)\right]^2} \\ &= e^{-\left(\frac{1}{2\sigma^2}\right)[\varepsilon_i - \mu]^2} \end{aligned} \tag{14}$$

with

$$\mu = \frac{\lambda_1}{\lambda_1 + \lambda_3} \varepsilon_{i-1} - \frac{\lambda_2}{2(\lambda_1 + \lambda_3)} \tag{15}$$

$$\sigma = \frac{1}{\sqrt{2(\lambda_1 + \lambda_3)}} \tag{16}$$

To quantify the relation between consecutive disturbances, we use affine Gaussian representation (Devroye, 1996) to recast the statistical expression into closed-form as:

$$\begin{aligned} \mathcal{E}_i &= \mu + \sigma Z_i = \frac{\lambda_1}{\lambda_1 + \lambda_3} \mathcal{E}_{i-1} - \frac{\lambda_2}{2(\lambda_1 + \lambda_3)} + \sigma Z_i \\ &= \omega \mathcal{E}_{i-1} + b + \sigma Z_i \end{aligned} \tag{17}$$

where $Z$ follows the standard normal distribution, i.e., $Z_i \sim \mathcal{N}(0,1)$ and $\omega$, $b$ denote the disturbance propagation coefficients for simplification:

$$\omega = \frac{\lambda_1}{\lambda_1 + \lambda_3} \tag{18}$$

$$b = -\frac{\lambda_2}{2(\lambda_1 + \lambda_3)} \tag{19}$$

Here, $\omega$ governs the amplification or attenuation of disturbances, and $\sigma$ captures stochastic variability. This equation directly characterizes how a disturbance at vehicle $(i-1)$ is transmitted to vehicle $i$, thereby describing propagation along successive leader-follower pairs in space. Noted that this is not intended as an exact finite-platoon joint process satisfying the sample-centering constraint of disturbances, but as an unconstrained local approximation to the conditional propagation for theoretical convenience.

According to this equation, speed disturbances propagate linearly along the platoon under each given density ($\lambda_1$ is a function of density $k$ and $\omega$ as well). By recursively expanding Eq. (17), the relation between any two speed disturbances at a distance of $m$ vehicles can be derived:

$$\mathcal{E}_{i+m} = \omega^m \mathcal{E}_i + \frac{1-\omega^m}{1-\omega} b + \sqrt{\frac{1-\omega^{2m}}{1-\omega^2}} \sigma Z_i \tag{20}$$

Remarkably, the derived growth pattern accords with previous empirical observations (Xu and Laval, 2019; S.-T. Zheng et al., 2022), which showed a concave growth of oscillation measured by the speed standard deviation of vehicles in the platoon. Consistently, the derived standard deviation of speed disturbances in Eq. (20), which is also the standard deviation of the speed, increases concavely along the platoon, as $\sqrt{\frac{1-\omega^{2m}}{1-\omega^2}}$ is a concave function of vehicle index $m$.

#### 4.2.2. *Response function of mean flow*

To quantify the collective response to speed disturbances, we also conduct the perturbative expansion on the joint distribution of speeds in the platoon. By substituting $V_i = \overline{V} + \mathcal{E}_i$ into the joint distribution in Eq. (6), we obtain the conditional distribution $P(\bar{V}|\boldsymbol{\mathcal{E}})$ under disturbances $\boldsymbol{\mathcal{E}} = (\mathcal{E}_0, \mathcal{E}_1, \cdots, \mathcal{E}_n)$ via a change of variables:

$$\begin{aligned} P(\bar{V} = \bar{v} | \boldsymbol{\mathcal{E}} = \boldsymbol{\varepsilon}) &\propto e^{-[\sum_{i=1}^n \lambda_1(\varepsilon_i - \varepsilon_{i-1})^2 + \sum_{i=1}^n \lambda_3 \varepsilon_i^2]} e^{-\lambda_2 n \bar{v}} \\ &\approx e^{-[\sum_{i=1}^n \lambda_1(\varepsilon_i - \varepsilon_{i-1})^2 + \sum_{i=1}^n \lambda_3 \varepsilon_i^2]} P(\bar{V} = \bar{v} | \boldsymbol{\mathcal{E}} = \mathbf{0}) \end{aligned} \tag{21}$$

where $P(\bar{V}|\boldsymbol{\mathcal{E}} = \mathbf{0})$ is a special case in equilibrium, which is the distribution of equilibrium speed $V_e$, i.e., $P(\bar{V}|\boldsymbol{\mathcal{E}} = \mathbf{0}) = P(V_e)$. Note that the approximate relationship between $P(\bar{V}|\boldsymbol{\mathcal{E}} = \boldsymbol{\varepsilon})$ and $P(\bar{V}|\boldsymbol{\mathcal{E}} = \mathbf{0})$ arises from the rough equivalence of their normalization factors.

Then the mean speed and the mean flow conditioned on disturbances are:

$$\mathrm{E}[\bar{V}|\boldsymbol{\mathcal{E}} = \boldsymbol{\varepsilon}] \approx e^{-[\sum_{i=1}^n \lambda_1(\varepsilon_i - \varepsilon_{i-1})^2 + \sum_{i=1}^n \lambda_3 \varepsilon_i^2]} \mathrm{E}[\bar{V}|\boldsymbol{\mathcal{E}} = \mathbf{0}] \tag{22}$$

$$\mathrm{E}[Q|\boldsymbol{\mathcal{E}} = \boldsymbol{\varepsilon}] \approx e^{-[\sum_{i=1}^n \lambda_1(\varepsilon_i - \varepsilon_{i-1})^2 + \sum_{i=1}^n \lambda_3 \varepsilon_i^2]} \mathrm{E}[Q|\boldsymbol{\mathcal{E}} = \mathbf{0}] \tag{23}$$

where $\mathrm{E}[Q|\boldsymbol{\mathcal{E}} = \mathbf{0}] = \mathrm{E}[Q_e]$ is the equilibrium mean flow, as in Eq. (10). Therefore, the response function of mean flow is derived as the relation between the equilibrium mean flow and the mean flow conditioned on disturbances. To align with Eq. (1), we further derive the expected flow drop magnitude $\delta$:

$$\delta \approx 1 - e^{-[\sum_{i=1}^n \lambda_1(\varepsilon_i - \varepsilon_{i-1})^2 + \sum_{i=1}^n \lambda_3 \varepsilon_i^2]} \tag{24}$$

Obviously, $\delta$ is positive with $\lambda_1 > 0$, $\lambda_3 > 0$ proved in our previous work, implying that flow rate will always drop under disturbances.

### 4.3. *Effective range of disturbance propagation*

Capacity drop results from the long-range propagation of speed disturbances, which we define as the effective spatial range of disturbance propagation. Within this effective range, traffic flow exhibits a collective response, while beyond it, disturbances and their corresponding responses become localized and uncorrelated. To quantify this effective range, we employ the concept of correlation length in the phase transition theory (Nishimori and Ortiz, 2010), see Fig. 4, based on which we capture the essential pattern of disturbance propagation and simplify the response function accordingly.

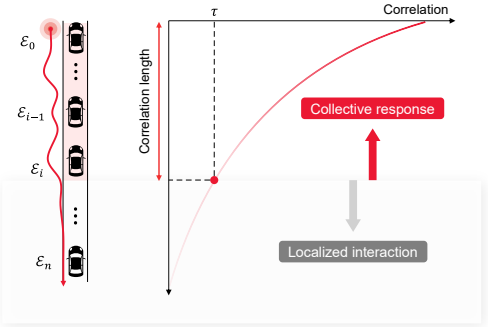



**Fig. 4.** Effective range of disturbance propagation quantified by the correlation length.

#### 4.3.1. *Introduction of correlation length*

The correlation length is a fundamental concept in statistical mechanics, which characterizes the spatial extent over which fluctuations or correlations in a system persist. It is widely utilized across disciplines including condensed matter physics (Chayes et al., 1986), biophysics (Cavagna et al., 2018), and signal processing (Lubow, 1968), playing a vital role in quantifying spatial correlations and understanding phase transitions, critical phenomena, and the behavior of complex systems.

Formally, the correlation length is defined through correlation function. For any two vehicles separated by a distance of $m$ vehicles at

Just Accepted

a given time window, the correlation function $C(m)$ is given by:

$$C(m) = \frac{\mathrm{E}[\sum_i (V_i - \bar{V})(V_{i+m} - \bar{V})]}{\mathrm{E}[\sum_i (V_i - \bar{V})^2]} \tag{25}$$

Typically, the correlation function is close to 1 with small $m$, and decays as $m$ increases. The correlation length $\xi_{veh}$ in units of vehicles is then defined as the characteristic length scale over which $C(m)$ decays, where $\tau$ is the correlation threshold and $\tau \to 0$.

$$C(\xi_{veh}) = \tau \tag{26}$$

Due to different decaying patterns in various systems, the correlation threshold can vary (e.g., $\tau = 1/e$ for exponential decay in Ising model of magnets (Newell and Montroll, 1953)). In this study, the correlation threshold serves as a parameter that requires calibration for simplicity.

#### *4.3.2. Derivation of correlation length*

The correlation length characterizes the effective propagation range of disturbances, and thus can be derived by analyzing the disturbances and their correlations. We first obtain the correlation function with respect to speed disturbances:

$$C(m) = \frac{\mathrm{E}[\sum_i \mathcal{E}_i \mathcal{E}_{i+m}]}{\mathrm{E}[\sum_i (\mathcal{E}_i)^2]} \tag{27}$$

By substituting the disturbance propagation equation of Eq. (20) into Eq. (27), we have:

$$C(m) = \frac{E\left[\sum_i \mathcal{E}_i \left(\omega^m \mathcal{E}_i + \frac{1-\omega^m}{1-\omega} b + \sqrt{\frac{1-\omega^{2m}}{1-\omega^2}} \sigma Z_i\right)\right]}{E[\sum_i (\mathcal{E}_i)^2]} \tag{28}$$

Expanding the numerator of Eq. (28) into three terms:

$$\mathrm{E}\left[\sum_i \omega^m (\mathcal{E}_i)^2\right] + \mathrm{E}\left[\sum_i \mathcal{E}_i \cdot \frac{1-\omega^m}{1-\omega} b\right] + \mathrm{E}\left[\sum_i \mathcal{E}_i \cdot \sqrt{\frac{1-\omega^{2m}}{1-\omega^2}} \sigma Z_i\right] \tag{29}$$

The second term of Eq. (29) vanishes, as $\mathrm{E}[\sum_i \mathcal{E}_i] = \mathrm{E}[\sum_i (V_i - \bar{V})] = \mathrm{E}[\sum_i V_i - n\bar{V}] = 0$ by the definition of speed disturbances:

$$\mathrm{E}\left[\sum_i \mathcal{E}_i \cdot \frac{1-\omega^m}{1-\omega} b\right] = \frac{1-\omega^m}{1-\omega} b \cdot \mathrm{E}\left[\sum_i \mathcal{E}_i\right] = 0 \tag{30}$$

The third term of Eq. (29) also vanishes since $Z_i$ is independent of $\mathcal{E}_i$ and $\mathrm{E}[Z_i] = 0$ by construction:

$$\mathrm{E}\left[\sum_i \mathcal{E}_i \cdot \sqrt{\frac{1-\omega^{2m}}{1-\omega^2}} \sigma Z_i\right] = \sqrt{\frac{1-\omega^{2m}}{1-\omega^2}} \sigma \cdot \mathrm{E}\left[\sum_i \mathcal{E}_i\right] \cdot \mathrm{E}[Z_i] = 0 \tag{31}$$

Therefore, only the first term of Eq. (29) survives, yielding:

$$C(m) = \frac{\mathrm{E}[\sum_i \omega^m (\mathcal{E}_i)^2]}{\mathrm{E}[\sum_i (\mathcal{E}_i)^2]} = \omega^m \tag{32}$$

Substituting Eq. (32) into Eq. (26), the correlation length is given as:

$$C(\xi_{veh}) = \omega^{\xi_{veh}} = \tau \tag{33}$$

Taking the natural logarithm and substituting $\omega$ from Eq. (18), we have:

$$\xi_{veh} = \ln \tau / \ln \omega = \ln \tau / [\ln \lambda_1 - \ln(\lambda_1 + \lambda_3)] \tag{34}$$

Based on the derived correlation length, we further constrain the response function to this range. Beyond the correlation length, the correlations of disturbances (i.e., disturbances propagation) become negligible and thus the collective response (i.e., effects of disturbances propagation) vanishes (Bialek et al., 2014). Therefore, the response function of mean flow, as in Eq. (23), should be confined within the correlation length:

$$\mathrm{E}[Q|\boldsymbol{\mathcal{E}} = \boldsymbol{\varepsilon}] \approx e^{-\left[\sum_{i=1}^{\xi_{veh}} \lambda_1 (\varepsilon_i - \varepsilon_{i-1})^2 + \sum_{i=1}^{\xi_{veh}} \lambda_3 (\varepsilon_i)^2\right]} \mathrm{E}[Q|\boldsymbol{\mathcal{E}} = \mathbf{0}] \tag{35}$$

The expected flow drop magnitude $\delta$ is then simplified as:

$$\delta \approx 1 - e^{-\left[\sum_{i=1}^{\xi_{veh}} \lambda_1 (\varepsilon_i - \varepsilon_{i-1})^2 + \sum_{i=1}^{\xi_{veh}} \lambda_3 (\varepsilon_i)^2\right]} \tag{36}$$

#### *4.4. Expected capacity drop magnitude at critical density*

In the canonical theory of phase transition, the critical point marking a sudden change in system properties is typically identified by analyzing the correlation length, which diverges near the critical point following a power-law behavior (Nishimori and Ortiz, 2010). However, in diverse real-world systems such as traffic flow, the correlation length remains bounded where traditional scaling laws may not directly apply. In such context, an alternative method to discern the critical point is to maximize the finite correlation length, which provides a pragmatic means to characterize critical phenomena (Cardy, 1996; Helbing, 2001).

Intuitively, before the critical density, in free-flow traffic, disturbances decay quickly due to ample spacing, resulting in a short correlation length. At the critical density, traffic becomes tightly coupled, and small disturbances can propagate over long distances, leading to a peak in correlation length. Beyond the critical density, in congested traffic, interactions become highly localized due to reduced speeds and tighter spacing, causing the correlation length to shorten again. Therefore, the maximum correlation length identifies the critical density (Hohenberg and Halperin, 1977).

Given that the correlation length commonly used to signify the critical point is measured in metric distance, we calculate the correlation length in meters, denoted as $\xi_l$:

$$\xi_l = 1000\, \xi_{veh}/k = 1000 \ln \tau / k[\ln \lambda_1 - \ln(\lambda_1 + \lambda_3)] \tag{37}$$

To derive the critical density $k_c$, we maximize the correlation length $\xi_l$:

$$k_c = \underset{k}{\operatorname{argmax}}\, \xi_l = \underset{k}{\operatorname{argmax}}\, k[\ln \lambda_1 - \ln(\lambda_1 + \lambda_3)] \tag{38}$$

By solving this optimization problem with respect to $k$, utilizing the relation between $\lambda_1$ and $k$ in Eq. (3), the critical density can be obtained. Eventually, the capacity drop at critical density is given by:

$$\delta_{k_c} \approx 1 - e^{-[\sum_{i=1}^{\xi_{veh}} \lambda_1 (\varepsilon_i - \varepsilon_{i-1})^2 + \sum_{i=1}^{\xi_{veh}} \lambda_3 (\varepsilon_i)^2]|_{k_c}} \tag{39}$$

Using the disturbance propagation equation in Eq. (20), the summation of disturbance terms can be further simplified to functions of initial disturbance $\varepsilon_0$:

$$\sum_{i=1}^{\xi_{veh}} (\varepsilon_i - \varepsilon_{i-1})^2 = \sum_{i=1}^{\xi_{veh}} \omega^{2(i-1)} (\varepsilon_1 - \varepsilon_0)^2 = \frac{1-\omega^{2\xi_{veh}}}{1-\omega^2} (\omega\varepsilon_0 + b - \varepsilon_0)^2 \tag{40}$$

$$\sum_{i=1}^{\xi_{veh}} (\varepsilon_i)^2 = \left(\omega\varepsilon_0{}^2 + \frac{\omega(\omega\varepsilon_0 + b - \varepsilon_0)}{1-\omega}\right) \frac{1-\omega^{\xi_{veh}}}{1-\omega} - \frac{\omega(\omega\varepsilon_0 + b - \varepsilon_0)}{1-\omega} \xi_{veh} \omega^{\xi_{veh}} \tag{41}$$

By substituting Eq. (38), Eq. (40), Eq. (41) into Eq. (39), we can derive the complete expression of expected capacity drop magnitude. To be concise, we only show its compact form as a function of influencing factors, where all the related variables and their expressions are summarized in Table 2 for easy reference:

$$\delta_{k_c} = f\left(\lambda_1(k_c), \lambda_3, \varepsilon_0, \omega(k_c), b(k_c), \xi_{veh}(k_c)\right) = f(\eta, \theta, \alpha, \beta, \lambda_3, \tau, \varepsilon_0) \tag{42}$$

**Table 2.** Variables in the capacity drop model.

| Module | Variable | | Expression |
|---|---|---|---|
| LFCD-STM | $\lambda_1$<br>$\lambda_2$<br>$\lambda_3$ | Lagrange multipliers | $\eta \ln k + \theta$<br>$\alpha \ln k + \beta$<br>$\lambda_3$ |
| Perturbative expansion | $\varepsilon_0$ | Initial speed disturbance | $\varepsilon_0$ |
| | $\omega$ | Disturbance propagation coefficients | $\lambda_1/(\lambda_1 + \lambda_3)$ |
| | $b$ | | $-\lambda_2/[2(\lambda_1 + \lambda_3)]$ |
| Correlation length | $\xi_{veh}$ | Correlation length (veh) | $\ln \tau/[\ln \lambda_1 - \ln(\lambda_1 + \lambda_3)]$ |
| | $\xi_l$ | Correlation length (m) | $\ln \tau/k[\ln \lambda_1 - \ln(\lambda_1 + \lambda_3)]$ |
| | $k_c$ | Critical density | $\underset{k}{\operatorname{argmax}}\, k[\ln \lambda_1 - \ln(\lambda_1 + \lambda_3)]$ |

Just Accepted

To illustrate the proposed capacity drop model intuitively, we further present the input-output flow in Fig. 5. The model connects the macroscopic capacity drop with microscopic behaviors through a concise yet effective formulation that focuses on disturbance propagation along the platoon.

External interruptions, such as LC, on-ramp merging, and sudden braking, are represented through two complementary pathways. First, an aggregated initial disturbance term $\varepsilon_0$, calibrated from empirical data, encodes the net effect of lateral interruptions and other exogenous shocks that are not explicitly resolved within a longitudinal platoon representation. Second, the stochastic propagation of disturbances, governed by the proposed leader-follower conditional distribution and its associated microscopic parameters $\eta, \theta, \alpha, \beta, \lambda_3$, captures how disturbances transmit and evolve longitudinally. Additionally, repeated or interacting perturbations may influence both components through their cumulative effects. By focusing on disturbance propagation along the platoon, which determines whether disturbances dissipate or amplify into sustained congestion, this formulation remains parsimonious while characterizing the essential physics of capacity drop.

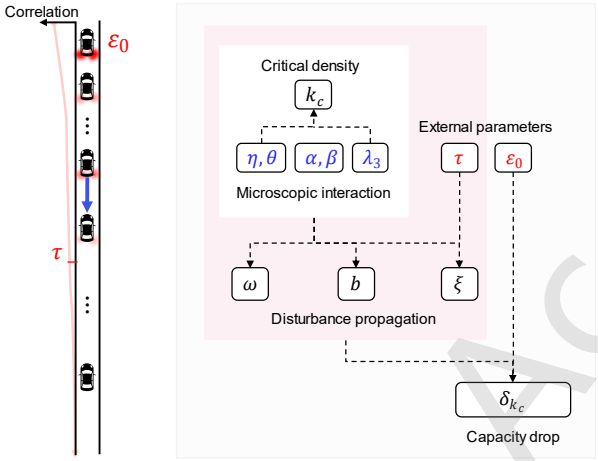



**Fig. 5.** Input-output flow of the proposed capacity drop model.

## 5 Validation

In this section, we validate the proposed capacity drop model using two carefully selected datasets: Zen and I-24 MOTION datasets. These datasets provide a comprehensive view of the capacity drop phenomenon while also representing different traffic environments, enabling a systematic evaluation of the model. The validation is conducted across scales: microscopic leader–follower interaction parameters are calibrated from trajectory data, while the resulting macroscopic capacity drop response is used to evaluate the proposed micro-to-macro analytical link. We first outline the methods of empirical analysis and model calibration, and then present the validation results.

### *5.1. Methods of empirical analysis and model calibration*

#### *5.1.1. Empirical analysis methods*

Since the aim of this paper is to link the microscopic disturbances to macroscopic capacity drop at critical density, we require the empirical measures of both capacity drop and critical density, as well as the empirical pattern of disturbance propagation for validation.

Empirical capacity drop is generally measured by the relative change in flow rate between free-flow states and congested states (Banks, 1991; Daganzo, 1997). To identify the traffic states, we apply wavelet transform to the speed profiles as per Z. Zheng et al. (2011). Specifically, the speed profile is sampled every 30 s and analyzed using the Mexican-hat continuous wavelet over physical scales of 1–10 min. The absolute wavelet coefficients are averaged across scales, and prominent interior peaks exceeding three median absolute deviations are identified as state transitions. To mitigate edge effects, one maximum wavelet scale is excluded at both boundaries, and the first and last admissible peaks determine the onset and recovery of congestion. Based on the identified states, we calculate the maximum flow rate in free flow states (i.e., the capacity) and the average flow rate in congested states (i.e., the QDF). The relative change in these flow rates is identified as the capacity drop magnitude (National Academies of Sciences, Engineering, and Medicine (NASEM), 2022). Due to the aggregation, the capacity drop magnitude can be viewed as the empirical expectation, which is consistent with our formulation.

Empirical critical density is typically determined by identifying the density range in the fundamental diagram (FD) where flow rate starts to decline as density increases, signaling the transition from free flow to congestion (Papageorgiou et al., 1991). However, it is difficult to pinpoint the exact value in FD due to the surge in stochasticity around this critical point. To locate the critical density more precisely, we calculate the correlation length and define the critical density at its peak, as the maximum correlation length corresponds to the critical point directly. Here we determine the empirical capacity drop and critical density separately, whereas the proposed model assumes that the capacity drop occurs at the critical density. This can be understood in a statistical sense that the capacity drop is deemed to occur at the critical density on average.

As for the empirical pattern of disturbance propagation, we extract the speed disturbances with the longest propagation range (maximum correlation length) at critical density for analysis. Specifically, we first retrieve the trajectory data within the time interval of critical density. By subtracting speeds from the platoon's average speed of this interval, we then obtain the speed disturbance of each vehicle. To explore the empirical propagation pattern of disturbances, which is modeled to propagate linearly for each density in this study, we further plot the disturbances against the vehicle index.

#### *5.1.2 Model calibration methods*

There are three parts of parameters in the proposed capacity drop model that require calibration, including the Lagrange multipliers $(\lambda_1, \lambda_2, \lambda_3)$ and their coefficients $(\eta, \theta, \alpha, \beta)$ within the LFCD-STM model, the correlation threshold $\tau$, and the initial disturbance $\varepsilon_0$.

For the parameters within the LFCD-STM model, we directly adopt the calibration methods in our previous work (X. Zhang et al., 2025). To be specific, we first calibrate the Lagrange multipliers $\lambda_1, \lambda_2, \lambda_3$ by employing maximum likelihood estimation:

$$\max_{(\lambda_1,\lambda_2,\lambda_3)} \ln \prod_j P\left(V_i = v_i^{(j)} \middle| V_{i-1} = v_{i-1}^{(j)}\right) \tag{43}$$

where the superscript of $(j)$ denotes the $j$th speed sample of the leader-follower pairs.

Given the relation between $\lambda_1, \lambda_2$ and spacing as in Eq. (3) and Eq. (4), we further obtain their coefficients $\eta, \theta$ and $\alpha, \beta$ respectively using the linear regression. Based solely on the calibrated LFCD-STM parameters, we first estimate the critical density using Eq. (38), independently of the correlation threshold $\tau$, which is subsequently calibrated by matching the empirical maximum correlation length at the estimated critical density.

Just Accepted

$$\tau = e^{k_c[\ln \lambda_1(k_c) - \ln(\lambda_1(k_c)+\lambda_3)] \max \xi_l} \quad (44)$$

To quantify the initial disturbance $\varepsilon_0$ at the critical point, which is regarded as the external perturbation arising from microscopic behaviors, we first extract the trajectory data during the time interval exhibiting the maximum correlation length. Within the initial frames, we identify the first vehicle whose speed drops below the platoon's average speed. The deviation between this vehicle's speed and the average speed is then determined as the initial disturbance.

With all the calibrated parameters, we thus can estimate the expected capacity drop magnitude with Eq. (39). We further compute the expected QDF using Eq. (1), with the expected capacity that maximizes the equilibrium flow in Eq. (10).

### *5.2. Experiments on Zen traffic dataset*

#### *5.2.1. Data description*

We first validate the capacity drop model using the Zen traffic dataset (Hanshin Expressway Company, 2023), which is a large-scale high-resolution trajectory dataset. The data utilized in this study were collected along the Hanshin Expressway Route 11 Ikeda Line during 10:00-11:00 am, with approximately 89% passenger cars and 11% large vehicles. As shown in Fig. 6, this isolated on-ramp bottleneck spans from Kilo Poster (KP) 4.20 to KP 3.65 with the Tsukamoto on-ramp, consisting of a left driving lane and a right passing lane. Noted that lane changes are prohibited in all lanes in this section. To avoid anomalous CF behaviors resulting from merging behaviors, we exclusively consider trajectory data in the right passing lane.

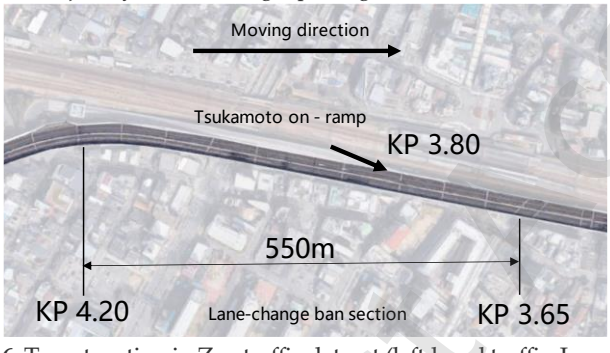



**Fig. 6.** Target section in Zen traffic dataset (left-hand traffic, Japan).

#### *5.2.2. Empirical analysis*

Following the empirical analysis methods, we first obtain the empirical capacity drop of Zen dataset. As shown in Fig. 7, we categorize traffic states using the wavelet transform and calculate the capacity in free flow states (1920 veh/h) and the QDF in congested states (1507 veh/h). The empirical capacity drop is then obtained as the relative change between these two flow rates, which is 21.5%.

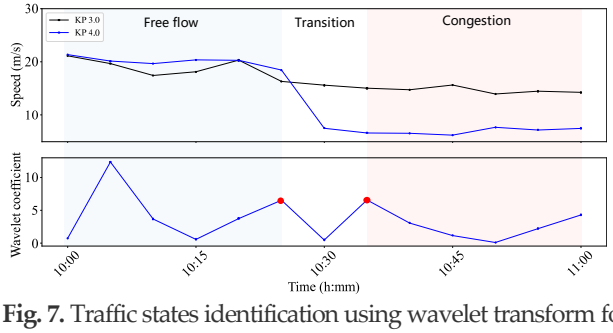
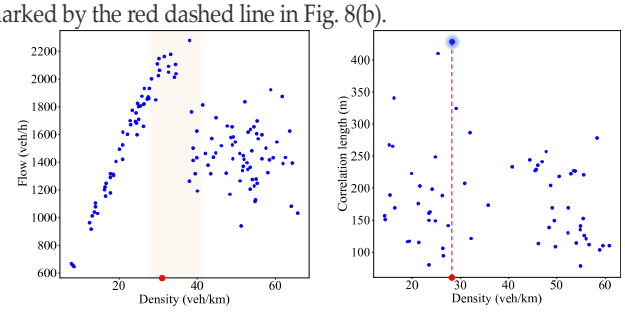



**Fig. 7.** Traffic states identification using wavelet transform for Zen dataset.

For the empirical critical density, it ranges from 26 to 40 veh/km according to the empirical FD aggregated in one minute, as highlighted with a red span in Fig. 8(a). Consistent with this potential range observed in the empirical FD, the empirical correlation length further identifies the critical density as 28.2 veh/km at its peak of 428.6 m, marked by the red dashed line in Fig. 8(b).




(a) Empirical FD (b) Empirical correlation length

**Fig. 8.** Empirical critical density determination for the Zen dataset.

We also obtain empirical speed disturbances propagating along the platoon at the critical density. As shown in Fig. 9, there is a linear relationship between leader's and follower's speed disturbances with a high $R^2$ value of 0.8, supporting the linear propagation under a given density in derived speed disturbance equation in Eq. (17).

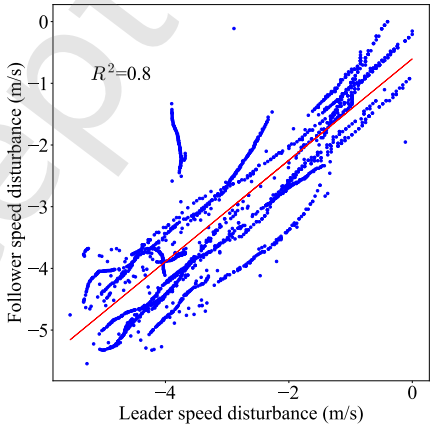



**Fig. 9.** Empirical speed disturbance propagation at critical density in Zen dataset.

#### *5.2.3. Validation results*

Utilizing the calibration methods, we calibrate all the parameters and summarize the results in Table 3.

**Table 3.** Calibrated parameters for Zen dataset.

| Parameters | | | Value |
|---|---|---|---|
| Lagrange multipliers | $\lambda_1$ | $\eta$ | 0.172 |
| | | $\theta$ | 0.768 |
| | $\lambda_2$ | $\alpha$ | 0.067 |
| | | $\beta$ | 0.218 |
| | $\lambda_3$ | | 0.051 |
| Initial disturbance | $\varepsilon_0$ | | -0.75 (m/s) |
| Correlation threshold | $\tau$ | | 0.033 |

Based on the calibrated parameters, we estimate the expected capacity drop magnitude and critical density, as well as the expected capacity and expected QDF. As presented in Table 4, the theoretical estimation shows a remarkable consistency with empirical results, where all the relative errors are below 5%, affirming the effectiveness of our capacity drop model.

Just accepted

**Table 4.** Validation results for Zen dataset.

| | Zen | Model estimation | Relative error |
|---|---|---|---|
| Critical density $k_c$ (veh/km) | 28.2 | 27.0 | 4.3% |
| Expected capacity (veh/h) | 1920 | 1917 | 0.1% |
| Expected QDF (veh/h) | 1507 | 1514 | 0.5% |
| Expected capacity drop magnitude $\delta_{k_c}$ | Zen | Model estimation | Absolute error |
| | 21.5% | 21.0% | 0.5% |

### *5.3. Experiments on I-24 MOTION dataset*

#### *5.3.1 Data description*

To further scrutinize the performance of the proposed model, another naturalistic vehicle trajectory dataset recorded on I-24 in the Nashville-Davidson County Metropolitan area using 4K resolution video cameras, I-24 MOTION dataset (Gloudemans et al., 2023), is utilized. This trajectory dataset covers a stretch of 4.2 miles (6.75 km) with 4-5 lanes in each direction and experiences regular recurring congestion. We choose the westbound trajectory data from 6 am to 10 am on Tuesday, 22 Nov, 2022, which includes morning peak hour conditions with heavy trucks comprising approximately 10-15% of total volume. The isolated bottleneck spanning 640 meters, situated between Mile Marker (MM) 58.8 and MM 59.2 with lane changing permitted, is further selected for capacity drop analysis. To avoid the impact of merging behaviors, we only use the data in lane 2, while the left-most lane 1 is a HOV (High-Occupancy Vehicle) lane. See Fig. 10 for a schematic illustration of the study area in I-24 MOTION.

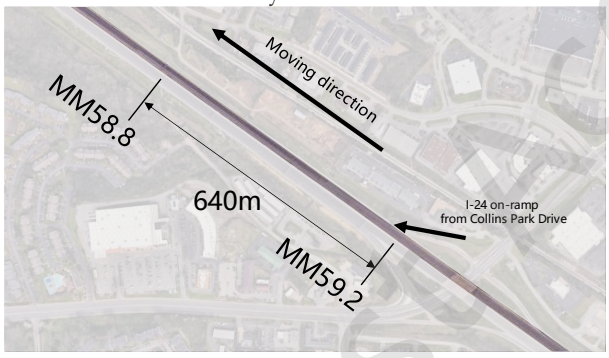



**Fig. 10.** Selected section in I-24 MOTION dataset.

#### *5.3.2. Empirical analysis*

Following the same procedure, we first identify different traffic states using wavelet transform, as shown in Fig. 11. With the empirical capacity in free flow (1776 veh/h) and the empirical QDF in congestion (1465 veh/h), we obtain the empirical capacity drop, which is 17.5%.

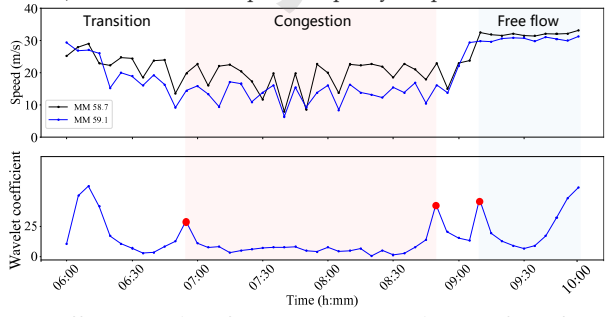
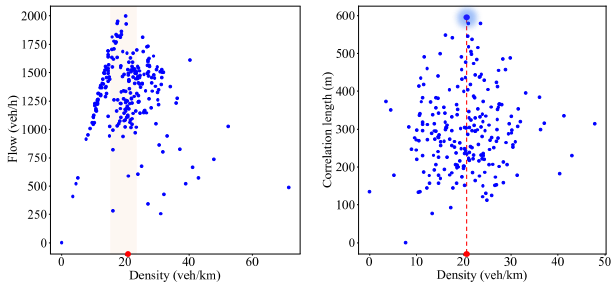



**Fig. 11.** Traffic states identification using wavelet transform for I-24 MOTION dataset.

Combining the empirical FD, the critical density for the I-24 MOTION dataset is determined as 20.7 veh/km with the maximum correlation length of 594.6 m, as shown in Fig. 12.




(a) Empirical FD (b) Empirical correlation length

**Fig. 12.** Empirical critical density determination for the I-24 MOTION dataset.

Moreover, we extract the empirical speed disturbances at critical density. As illustrated in Fig. 13, the disturbances also exhibit a linear propagation between leader-follower pairs with a high $R^2$ of 0.9, which further validates the proposed disturbance propagation equation.

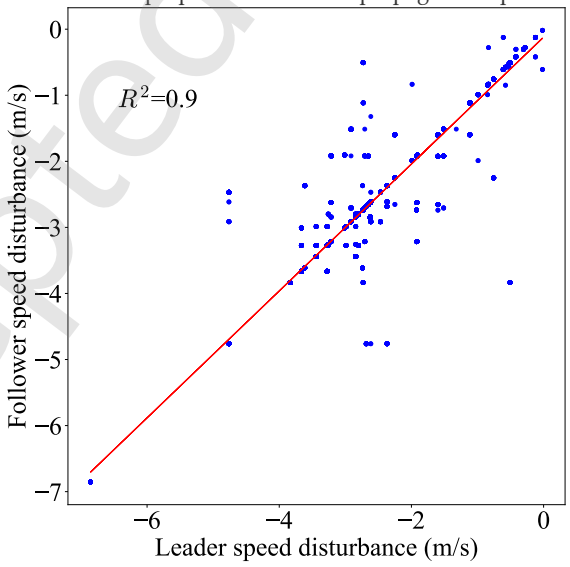



**Fig. 13.** Empirical speed disturbance propagation at critical density in I-24 MOTION dataset.

#### *5.3.3. Validation results*

Following the same calibration steps, Table 5 summarizes the calibrated parameters for I-24 MOTION. Using these calibrated parameters, we obtain the validation results presented in Table 6. From the table, we can see that the proposed model accurately estimates the critical density, expected capacity and QDF, with a maximum relative error of 2.5%. This further ensures high consistency in the expected capacity drop magnitude, which justifies the proposed capacity drop model.

**Table 5.** Calibrated parameters for I-24 MOTION dataset.

| Parameters | | | Value |
|---|---|---|---|
| Lagrange multipliers | $\lambda_1$ | $\eta$ | 0.087 |
| | | $\theta$ | 0.418 |
| | $\lambda_2$ | $\alpha$ | 0.087 |
| | | $\beta$ | 0.329 |
| | $\lambda_3$ | | 0.009 |
| Initial disturbance | $\varepsilon_0$ | | -1.41 (m/s) |
| Correlation threshold | $\tau$ | | 0.278 |

Under Accepted

**Table 6.** Validation results for I-24 MOTION dataset.

| | I-24 MOTION | Model estimation | Relative error |
|---|---|---|---|
| Critical density $k_c$ (veh/km) | 20.7 | 20.7 | 0% |
| Expected capacity (veh/h) | 1776 | 1731 | 2.5% |
| Expected QDF (veh/h) | 1465 | 1467 | 0.1% |
| | I-24 MOTION | Model estimation | Absolute error |
| Expected capacity drop magnitude $\delta_{k_c}$ | 17.5% | 15.3% | 2.3% |

## 6 Sensitivity analysis

### *6.1. Parameter sensitivity*

To demonstrate how the expected capacity drop magnitude can be altered by changing the parameters, we conduct sensitivity analysis on all the parameters $(\eta, \theta, \alpha, \beta, \lambda_3, \tau, \varepsilon_0)$ in the derived capacity drop model, where $\eta, \theta, \alpha, \beta, \lambda_3$ govern the leader-follower interaction and $\tau, \varepsilon_0$ are considered external parameters.

We first present the sensitivity analysis of $\eta, \theta, \alpha, \beta, \lambda_3$ in Fig. 14. Amongst these parameters, $\eta$ emerges as the most significant, where increasing $\eta$ alleviates the capacity drop, while $\lambda_3$ has a negligible impact.

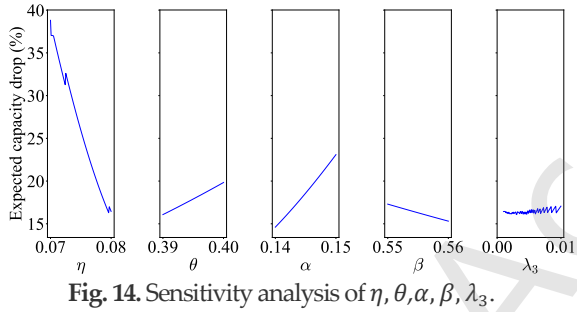



**Fig. 14.** Sensitivity analysis of $\eta, \theta, \alpha, \beta, \lambda_3$.

The impacts of the other two external parameters $\tau, \varepsilon_0$ on the expected capacity drop magnitude are illustrated in Fig. 15. From the figure, we can see that a smaller correlation threshold $\tau$ that extends the correlation length, namely a longer-range propagation of disturbances, leads to a larger capacity drop. A larger initial speed disturbance $\varepsilon_0$ (e.g., harder brake) also results in a more severe capacity drop as expected.

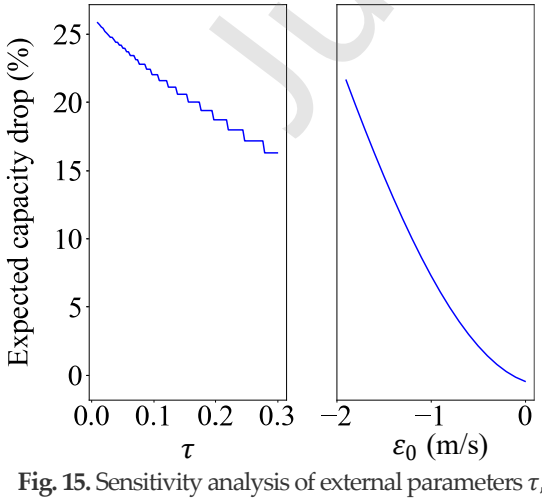



**Fig. 15.** Sensitivity analysis of external parameters $\tau, \varepsilon_0$.

On the other hand, we also investigate the influential factors $\eta, \theta, \lambda_3$ of critical density, which is essential for traffic control (e.g., ramp metering). As can be seen from Fig. 16, the critical density is more sensitive to changes in $\eta$ while exhibiting steadier responses to variations in $\theta$ and $\lambda_3$. Again, $\eta$ emerges as the most significant parameter for critical density.

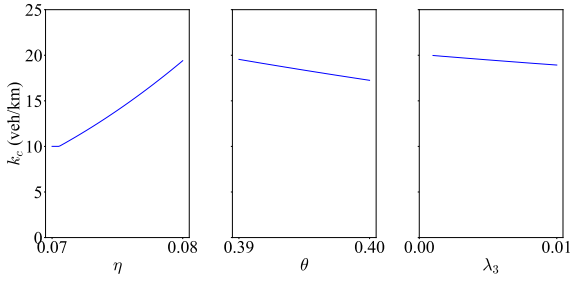



**Fig. 16.** Impacts of parameters on critical density.

### *6.2. Physical interpretation of the key parameter*

To gain more insights of the parameter $\eta$, which is important for both the capacity drop magnitude and critical density, we interpret it using the CF-like dynamic model of the proposed leader-follower conditional distribution according to the Brownian dynamics (Schlick, 2010), where $B(t)$ is the Brownian motion:

$$\begin{aligned}\frac{dv_i(t)}{dt} &= \nabla_{V_i} \log P\left(V_i(t)|V_{i-1}(t)\right) + \sqrt{2}B(t) \\ &= -2\lambda_1(v_i - v_{i-1}) - \lambda_2 - 2\lambda_3(v_i - \bar{v}) + \sqrt{2}B(t)\end{aligned} \tag{45}$$

We then obtain the partial derivative of acceleration in terms of the speed difference, while the random term is ignored for simplicity:

$$\frac{\partial a_i}{\partial \Delta v_i} \approx -2\lambda_1 \tag{46}$$

where $a_i$ denotes the acceleration of the subject vehicle, $\Delta v_i = v_i - v_{i-1}$ is the speed difference, and others have the same meanings as introduced before.

With the relation between $\lambda_1$ and $\eta$ in Eq. (3), we have:

$$\frac{\partial \lambda_1}{\partial s_i} = \frac{\partial(-\eta \ln s_i + \theta)}{\partial s_i} = \frac{-\eta}{s_i} \geq \frac{-\eta}{s_{min}} = -\eta \tag{47}$$

where the minimum distance is set to $s_{min} = 1\ m$ and $\eta > 0$.

Substituting Eq. (46) into Eq. (47), a possible interpretation of $\eta$ is:

$$\eta \geq -\frac{\partial \lambda_1}{\partial s_i} = \frac{1}{2}\frac{\partial^2 a_i}{\partial s_i \partial \Delta v_i} \Rightarrow \eta = \frac{1}{2}\max\left|\frac{\partial^2 a_i}{\partial s_i \partial \Delta v_i}\right| \tag{48}$$

Therefore, we can infer that $\eta$ is associated with the second-order partial derivative of acceleration with respect to speed difference and spacing, and a higher sensitivity of this second-order partial derivative (e.g., agile driving style) leads to more robust traffic flow with lower capacity drop and higher critical density.

These sensitivity results provide practical implications for traffic management and vehicle control. Larger initial disturbances and longer disturbance-correlation ranges both intensify capacity drop, suggesting that mitigation should suppress severe local disturbances and limit their propagation before traffic reaches the critical state. Traffic management measures such as ramp metering and speed harmonization can help avoid this critical regime, while appropriately designed connected and automated vehicle (CAV) control can attenuate disturbance propagation and improve traffic-flow resilience.

## 7 Conclusion

Despite the paramount importance of capacity drop in traffic flow theory and operation, an explicit link from microscopic interactions to this macroscopic phenomenon remains elusive. To address this gap, we analytically model the capacity drop from the perspective of speed

Just Accepted

disturbance propagation. Leveraging phase transition and critical phenomena theory, we demonstrate how disturbances propagating across the platoon at critical density culminates in the collective response of capacity drop.

Specifically, microscopic behaviors such as LC and variable CF generate speed disturbances. These disturbances propagate along the platoon, which is mainly governed by longitudinal interactions and further characterized by the correlation length. Beyond the correlation length, disturbances become uncorrelated and localized, while within it, traffic flow exhibits a collective response. This collective response becomes significant as the correlation length reaches its peak at the critical point, resulting in the capacity drop at the critical density.

Based on this idea, we derive the analytical model for capacity drop from the perspective of stochastic disturbance propagation. Specifically, by extending the LFCD-STM to non-equilibrium states through perturbation expansion, we first derive disturbance propagation equation and the response function of mean flow under disturbances. We then introduce the correlation length to quantify the effective range of disturbance propagation and the corresponding collective response. By confining the mean flow response function within the maximum correlation length, we obtain the expected capacity drop magnitude at the critical density. Using Zen and I-24 MOTION datasets, we calibrate and evaluate the proposed model, which demonstrates satisfactory performance with a relative error of less than 5% in critical density and flow rates.

Our findings reveal the effects of disturbance propagation in the capacity drop and analytically bridge the gap between them, offering actionable insights for traffic management and CAV deployment. Estimating critical density from trajectory data enables proactive control measures such as dynamic ramp metering, while minimizing disturbance correlation within CAV platoons and tuning the second-order acceleration sensitivity parameter ($\eta$) can further enhance traffic efficiency and resilience. Future research could explore the non-equilibrium dynamics of mixed traffic flow involving human-driven vehicles and CAVs.

## Replication and Data Sharing

Processed car-following data in Parquet format and analysis code are available at https://github.com/tjzxh/Capacity-Drop-Modeling-via-Stochastic-Disturbance-Propagation and https://ets-data.sciopen.com/ETSD.2026.9190112.


## Acknowledgements

This research is funded by the National Natural Science Foundation of China (52602554, 52125208, 52402374, T2588101), the Fundamental Research Funds for the Central Universities, and the Fundamental and Interdisciplinary Disciplines Breakthrough Plan of the Ministry of Education of China (No. JYB2025XDXM123), the National Engineering Research Center of Road Safety Control Technology (No. 2025GCZXKFKT19A).


## Appendix

To better understand the concept in probabilistic modeling, random variables are treated as discrete random variables in this paper, since the probability density function used to characterize a continuous random variable is more obscure. Note that these random variables can be regarded to be discretized with a very small step, thus there is no essential difference between the continuous and discrete type.

| Name | Notation | Name | Notation |
|---|---|---|---|
| Random variables | | Variables | |
| Speed of vehicle $i$ | $V_i$ | Expected flow drop and capacity drop magnitude | $\delta, \delta_{k_c}$ |
| Average speed of the platoon | $\overline{V}$ | Disturbance propagation coefficients | $\omega, b$ |
| Equilibrium speed and flow | $V_e, Q_e$ | Correlation length in meters and in vehicle numbers | $\xi_l, \xi_{veh}$ |
| Flow | $Q$ | Density and critical density | $k, k_c$ |
| Speed disturbance of vehicle $i$ | $\mathcal{E}_i$ | Total number of vehicles in the study section | $n$ |
| Speed disturbance vector | $\boldsymbol{\mathcal{E}}$ | Lagrange multipliers | $\lambda_1, \lambda_2, \lambda_3$ |
| Functions | | Parameters | |
| Correlation function between $m$ vehicles | $C(m)$ | Length of the study area, Maximum speed | $l, v_{max}$ |
| Normalization factor | $z$ | Regression parameters of the logarithm relationship | $\eta, \theta, \alpha, \beta$ |
| Brownian motion | $B(t)$ | Initial speed disturbance | $\varepsilon_0$ |
| | | Correlation threshold | $\tau$ |

## Author contributions

Xiaohui Zhang: Conceptualization, Methodology, Software, Validation, Writing-Original draft. Jie Sun: Conceptualization, Methodology, Validation, Writing-Reviewing and Editing. Jian Sun: Conceptualization, Methodology, Validation, Writing-Reviewing and Editing, Funding Acquisition. Yunpeng Wang: Funding acquisition.

## Declaration of competing interest

The authors have no competing interests to declare that are relevant to the content of this article.

Just Accepted

## References


Banks, J.H., 1991. Two-capacity phenomenon at freeway bottlenecks: A basis for ramp metering? Transportation Research Record 1320, 83–90.

Bertini, R.L., Leal, M.T., 2005. Empirical Study of Traffic Features at a Freeway Lane Drop. Journal of Transportation Engineering 131, 397–407. https://doi.org/10.1061/(ASCE)0733-947X(2005)131:6(397)

Bialek, W., Cavagna, A., Giardina, I., Mora, T., Silvestri, E., Viale, M., et al., 2012. Statistical mechanics for natural flocks of birds. Proceedings of the National Academy of Sciences 109, 4786–4791. https://doi.org/10.1073/pnas.1118633109

Bialek, W., Cavagna, A., Giardina, I., Mora, T., Pohl, O., Silvestri, E., et al., 2014. Social interactions dominate speed control in poising natural flocks near criticality. Proceedings of the National Academy of Sciences 111, 7212–7217. https://doi.org/10.1073/pnas.1324045111

Brackstone, M., McDonald, M., 1999. Car-following: a historical review. Transportation Research Part F: Traffic Psychology and Behaviour 2, 181–196. https://doi.org/10.1016/S1369-8478(00)00005-X

Brilon, W., Geistefeldt, J., Regler, M., 2005. Reliability of Freeway Traffic Flow: A stochastic Concept of Capacity. In: Proceedings of the 16th International Symposium on Transportation and Traffic Theory. Elsevier, pp. 125–144. https://doi.org/10.1016/B978-008044680-6/50009-X

Cáceres, M.O., 2017. Non-equilibrium Statistical Physics with Application to Disordered Systems. Springer International Publishing, Cham. https://doi.org/10.1007/978-3-319-51553-3

Cardy, J., 1996. Scaling and Renormalization in Statistical Physics. Cambridge University Press. https://doi.org/10.1017/CBO9781316036440

Cassidy, M.J., Bertini, R.L., 1999. Some traffic features at freeway bottlenecks. Transportation Research Part B: Methodological 33, 25–42. https://doi.org/10.1016/S0191-2615(98)00023-X

Cassidy, M.J., Rudjanakanoknad, J., 2005. Increasing the capacity of an isolated merge by metering its on-ramp. Transportation Research Part B: Methodological 39, 896–913. https://doi.org/10.1016/j.trb.2004.12.001

Castillo, J.M. del, 2001. Propagation of perturbations in dense traffic flow: a model and its implications. Transportation Research Part B: Methodological 35, 367–389. https://doi.org/10.1016/S0191-2615(99)00055-7

Cavagna, A., Giardina, I., Grigera, T.S., 2018. The physics of flocking: Correlation as a compass from experiments to theory. Physics Reports 728, 1–62. https://doi.org/10.1016/j.physrep.2017.11.003

Chandler, R.E., Herman, R., Montroll, E.W., 1958. Traffic Dynamics: Studies in Car Following. Operations Research 6, 165–184. https://doi.org/10.1287/opre.6.2.165

Chayes, J.T., Chayes, L., Fisher, D.S., Spencer, T., 1986. Finite-Size Scaling and Correlation Lengths for Disordered Systems. Physical Review Letters 57, 2999–3002. https://doi.org/10.1103/PhysRevLett.57.2999

Chen, D., Ahn, S., Laval, J., Zheng, Z., 2014. On the periodicity of traffic oscillations and capacity drop: The role of driver characteristics. Transportation Research Part B: Methodological 59, 117–136. https://doi.org/10.1016/j.trb.2013.11.005

Chen, D., Ahn, S., 2018. Capacity-drop at extended bottlenecks: Merge, diverge, and weave. Transportation Research Part B: Methodological 108, 1–20. https://doi.org/10.1016/j.trb.2017.12.006

Chen, D., Srivastava, A., Ahn, S., Li, T., 2019. Traffic dynamics under speed disturbance in mixed traffic with automated and non-automated vehicles. Transportation Research Procedia 38, 709–729. https://doi.org/10.1016/j.trpro.2019.05.037

Chowdhury, D., Santen, L., Schadschneider, A., 2000. Statistical physics of vehicular traffic and some related systems. Physics Reports 329, 199–329. https://doi.org/10.1016/S0370-1573(99)00117-9

Chung, K., Rudjanakanoknad, J., Cassidy, M.J., 2007. Relation between traffic density and capacity drop at three freeway bottlenecks. Transportation Research Part B: Methodological 41, 82–95. https://doi.org/10.1016/j.trb.2006.02.011

Coifman, B., 2015. Empirical flow-density and speed-spacing relationships: Evidence of vehicle length dependency. Transportation Research Part B: Methodological 78, 54–65. https://doi.org/10.1016/J.TRB.2015.04.006

Csiszar, I., 1991. Why Least Squares and Maximum Entropy? An Axiomatic Approach to Inference for Linear Inverse Problems. The Annals of Statistics 19, 2032–2066. https://doi.org/10.1214/aos/1176348385

Daganzo, C.F., 1997. Fundamentals of Transportation and Traffic Operations. Pergamon, Oxford.

Daganzo, C.F., 2002. A behavioral theory of multi-lane traffic flow. Part I: Long homogeneous freeway sections. Transportation Research Part B: Methodological 36, 131–158. https://doi.org/10.1016/S0191-2615(00)00042-4

Devroye, L., 1996. Random variate generation in one line of code, in: Proceedings of the 28th Conference on Winter Simulation - WSC '96. ACM Press, New York, New York, USA, pp. 265–272. https://doi.org/10.1145/256562.256623

Edie, L.C., 1961. Car-Following and Steady-State Theory for Noncongested Traffic. Operations Research 9, 66–76. https://doi.org/10.1287/opre.9.1.66

Gloudemans, D., Wang, Y., Ji, J., Zachár, G., Barbour, W., Hall, E., et al., 2023. I-24 MOTION: An instrument for freeway traffic science. Transportation Research Part C: Emerging Technologies 155, 104311. https://doi.org/10.1016/j.trc.2023.104311

Hall, F.L., Agyemang-Duah, K., 1991. Freeway capacity drop and the definition of capacity. Transportation Research Record 1320, 91–98.

Han, Y., Ahn, S., 2018. Stochastic modeling of breakdown at freeway merge bottleneck and traffic control method using connected automated vehicle. Transportation Research Part B: Methodological 107, 146–166. https://doi.org/10.1016/j.trb.2017.11.007

Han, Y., Wu, J., Ding, F., Li, Z., Liu, P., Leclercq, L., 2025. Capacity drop at active bottlenecks: An empirical study based on trajectory data. Transportation Research Part B: Methodological 196, 103218. https://doi.org/10.1016/j.trb.2025.103218

Hanshin Expressway Company, 2023. ZTD/Zen Traffic Data [WWW Document]. URL https://zen-traffic-data.net/english/ (accessed 5.6.24).

Helbing, D., 2001. Traffic and related self-driven many-particle systems. Reviews of Modern Physics 73, 1067–1141. https://doi.org/10.1103/RevModPhys.73.1067

Herman, R., Montroll, E.W., Potts, R.B., Rothery, R.W., 1959. Traffic


JSTA Accepted

Dynamics: Analysis of Stability in Car Following. Operations Research 7, 86–106. https://doi.org/10.1287/opre.7.1.86

Hohenberg, P.C., Halperin, B.I., 1977. Theory of dynamic critical phenomena. Reviews of Modern Physics 49, 435–479. https://doi.org/10.1103/RevModPhys.49.435

Jaynes, E.T., 1957. Information Theory and Statistical Mechanics. Physical Review 106, 620–630. https://doi.org/10.1103/PhysRev.106.620

Jaynes, E.T., 1982. On the rationale of maximum-entropy methods. Proceedings of the IEEE 70, 939–952. https://doi.org/10.1109/PROC.1982.12425

Jin, W.-L., Gan, Q.-J., Lebacque, J.-P., 2015. A kinematic wave theory of capacity drop. Transportation Research Part B: Methodological 81, 316–329. https://doi.org/10.1016/j.trb.2015.07.020

Jin, W.-L., 2017. A first-order behavioral model of capacity drop. Transportation Research Part B: Methodological 105, 438–457. https://doi.org/10.1016/j.trb.2017.09.021

Kerner, B.S., Klenov, S.L., Schreckenberg, M., 2011. Simple cellular automaton model for traffic breakdown, highway capacity, and synchronized flow. Physical Review E 84, 046110. https://doi.org/10.1103/PhysRevE.84.046110

Laval, J.A., Daganzo, C.F., 2006. Lane-changing in traffic streams. Transportation Research Part B: Methodological 40, 251–264. https://doi.org/10.1016/j.trb.2005.04.003

Leclercq, L., Laval, J.A., Chiabaut, N., 2011. Capacity Drops at Merges: an endogenous model. Procedia - Social and Behavioral Sciences 17, 12–26. https://doi.org/10.1016/j.sbspro.2011.04.505

Lubow, B., 1968. Correlation Entering New Fields with Real-Time Signal Analysis. IEEE Transactions on Electromagnetic Compatibility EMC-10, 284–284. https://doi.org/10.1109/TEMC.1968.302964

Marini Bettolo Marconi, U., Puglisi, A., Rondoni, L., Vulpiani, A., 2008. Fluctuation–dissipation: Response theory in statistical physics. Physics Reports 461, 111–195. https://doi.org/10.1016/j.physrep.2008.02.002

National Academies of Sciences, Engineering, and Medicine, 2022. Highway Capacity Manual 7th Edition: A Guide for Multimodal Mobility Analysis. The National Academies Press, Washington, DC. https://doi.org/10.17226/26432

Newell, G.F., Montroll, E.W., 1953. On the Theory of the Ising Model of Ferromagnetism. Reviews of Modern Physics 25, 159–159. https://doi.org/10.1103/RevModPhys.25.159

Ngoduy, D., Liu, R., 2007. Multiclass first-order simulation model to explain non-linear traffic phenomena. Physica A: Statistical Mechanics and its Applications 385, 667–682. https://doi.org/10.1016/j.physa.2007.07.041

Nishimori, H., Ortiz, G., 2010. Elements of Phase Transitions and Critical Phenomena. Oxford University Press, Oxford. https://doi.org/10.1093/acprof:oso/9780199577224.001.0001

Nishinari, K., Treiber, M., Helbing, D., 2003. Interpreting the wide scattering of synchronized traffic data by time gap statistics. Physical Review E 68, 067101. https://doi.org/10.1103/PhysRevE.68.067101

Oh, S., Yeo, H., 2015. Impact of stop-and-go waves and lane changes on discharge rate in recovery flow. Transportation Research Part B: Methodological 77, 88–102. https://doi.org/10.1016/j.trb.2015.03.017

Papageorgiou, M., Hadj-Salem, H., Blosseville, J.M., 1991. ALINEA: A local feedback control law for on-ramp metering. Transportation Research Record 1320, 58-64.

Papageorgiou, M., Papamichail, I., Spiliopoulou, A.D., Lentzakis, A.F., 2008. Real-time merging traffic control with applications to toll plaza and work zone management. Transportation Research Part C: Emerging Technologies 16, 535–553. https://doi.org/10.1016/j.trc.2007.11.002

Qian, W.-L., Siqueira, A.F., Machado, R.F., Lin, K., Grant, T.W., 2017. Dynamical capacity drop in a nonlinear stochastic traffic model. Transportation Research Part B: Methodological 105, 328-339. https://doi.org/10.1016/j.trb.2017.09.017

Schlick, T., 2010. Molecular Modeling and Simulation: An Interdisciplinary Guide, 2nd ed. Interdisciplinary Applied Mathematics, vol. 21. Springer, New York, NY. https://doi.org/10.1007/978-1-4419-6351-2

Shore, J., Johnson, R., 1980. Axiomatic derivation of the principle of maximum entropy and the principle of minimum cross-entropy. IEEE Transactions on Information Theory 26, 26–37. https://doi.org/10.1109/TIT.1980.1056144

Srivastava, A., Geroliminis, N., 2013. Empirical observations of capacity drop in freeway merges with ramp control and integration in a first-order model. Transportation Research Part C: Emerging Technologies 30, 161–177. https://doi.org/10.1016/j.trc.2013.02.006

Sun, J., Zheng, Z., Sun, J., 2018. Stability analysis methods and their applicability to car-following models in conventional and connected environments. Transportation Research Part B: Methodological 109, 212–237. https://doi.org/10.1016/j.trb.2018.01.013

Sun, J., Zheng, Z., Sun, J., 2020. The relationship between car following string instability and traffic oscillations in finite-sized platoons and its use in easing congestion via connected and automated vehicles with IDM based controller. Transportation Research Part B: Methodological 142, 58–83. https://doi.org/10.1016/j.trb.2020.10.004

Swaroop, D., Hedrick, J.K., 1996. String stability of interconnected systems. IEEE Transactions on Automatic Control 41, 349–357. https://doi.org/10.1109/9.486636

Treiber, M., Kesting, A., Helbing, D., 2006. Understanding widely scattered traffic flows, the capacity drop, and platoons as effects of variance-driven time gaps. Physical Review E 74, 016123. https://doi.org/10.1103/PhysRevE.74.016123

Treiber, M., Kesting, A., 2013. Traffic Flow Dynamics: Data, Models and Simulation. Springer, Berlin, Heidelberg. https://doi.org/10.1007/978-3-642-32460-4

Wilson, R.E., Ward, J.A., 2011. Car-following models: fifty years of linear stability analysis – a mathematical perspective. Transportation Planning and Technology 34, 3–18. https://doi.org/10.1080/03081060.2011.530826

Xu, T., Laval, J.A., 2019. Analysis of a Two-Regime Stochastic Car-Following Model: Explaining Capacity Drop and Oscillation Instabilities. Transportation Research Record: Journal of the Transportation Research Board 2673, 610–619. https://doi.org/10.1177/0361198119850464

Yuan, K., Knoop, V.L., Hoogendoorn, S.P., 2017. A Microscopic

Just Accepted

Investigation Into the Capacity Drop: Impacts of Longitudinal Behavior on the Queue Discharge Rate. Transportation Science 51, 852–862. https://doi.org/10.1287/trsc.2017.0745

Yuan, K., Laval, J., Knoop, V.L., Jiang, R., Hoogendoorn, S.P., 2019. A geometric Brownian motion car-following model: towards a better understanding of capacity drop. Transportmetrica B: Transport Dynamics 7, 915–927. https://doi.org/10.1080/21680566.2018.1518169

Zhang, X., Jarrett, D.F., 1997. Stability analysis of the classical car-following model. Transportation Research Part B: Methodological 31, 441–462. https://doi.org/10.1016/S0191-2615(97)00006-4

Zhang, H.M., Kim, T., 2005. A car-following theory for multiphase vehicular traffic flow. Transportation Research Part B: Methodological 39, 385–399. https://doi.org/10.1016/j.trb.2004.06.005

Zhang, C., Wang, W., Sun, L., 2024. Calibrating car-following models via Bayesian dynamic regression. Transportation Research Part C: Emerging Technologies 168, 104719. https://doi.org/10.1016/j.trc.2024.104719

Zhang, X., Sun, J., Zheng, Z., Sun, J., 2024. On the string stability of neural network-based car-following models: A generic analysis framework. Transportation Research Part C: Emerging Technologies 160, 104525. https://doi.org/10.1016/j.trc.2024.104525

Zhang, X., Sun, J., Sun, J., 2025. On the stochastic fundamental diagram: A general micro-macroscopic traffic flow modeling framework. Communications in Transportation Research 5, 100163. https://doi.org/10.1016/j.commtr.2025.100163

Zhang, C., He, Z., Wu, C., Sun, L., 2026. When context is not enough: Modeling unexplained variability in car-following behavior. Transportation Research Part B: Methodological 214, 103588. https://doi.org/10.1016/j.trb.2026.103588

Zheng, Z., Ahn, S., Chen, D., Laval, J., 2011. Applications of wavelet transform for analysis of freeway traffic: Bottlenecks, transient traffic, and traffic oscillations. Transportation Research Part B: Methodological 45, 372–384. https://doi.org/10.1016/j.trb.2010.08.002

Zheng, S.-T., Jiang, R., Tian, J., Li, X., Treiber, M., Li, Z.-H., et al., 2022. Empirical and experimental study on the growth pattern of traffic oscillations upstream of fixed bottleneck and model test. Transportation Research Part C: Emerging Technologies 140, 103729. https://doi.org/10.1016/j.trc.2022.103729

## Author biography



**Xiaohui Zhang** received her Ph.D. degree in Transportation Engineering from Tongji University in 2025. She is currently an assistant Professor in Institute of Smart City and Intelligent Transportation, Southwest Jiaotong University. Her main research interests include traffic flow theory and modeling and emerging technology for intelligent traffic system integrated machine learning.



**Jie Sun** received his Ph.D. degree in Transportation Engineering from Tongji University in 2019. He is currently working as an Associate Professor at Tongji University. He worked as a Postdoctoral Research Fellow at the University of Queensland and The Hong Kong University of Science and Technology, respectively. His main research interests include traffic flow theory and modeling, traffic simulation, and connected and automated vehicles.



**Jian Sun** received his Ph.D. degree from Tongji University in 2006. Subsequently, he was at Tongji University as a Lecturer and then promoted to the position of Professor in 2011, where he is currently a Professor with the College of Transportation Engineering and the Dean of the Department of Traffic Engineering. His main research interests include traffic flow theory, traffic simulation, connected and automated vehicles, and intelligent transportation systems.



**Yunpeng Wang** is a Professor at the School of Transportation Science and Engineering, Beihang University, and a member of the Chinese Academy of Engineering, elected in 2021. His research interests include vehicle safety monitoring, network-wide cooperative control, and integrated vehicle-infrastructure control.

Just Accepted